IEEE Access
Multidisciplinary | Rapid Review | Open Access Journal

Received March 8, 2019, accepted March 18, 2019, date of publication March 25, 2019, date of current version April 11, 2019.

Digital Object Identifier 10.1109/ACCESS.2019.2907159

Automatic Modulation Recognition of Radar Signals Based on Manhattan Distance-Based Features

YINGKUN HUANG, WEIDONG JIN, BING LI, PENG GE, AND YUNPU WU
College of Electrical Engineering, Southwest Jiaotong University, Chengdu 610031, China

Corresponding author: Weidong Jin (wdjin@home.swjtu.edu.cn)

This work was supported in part by the Fundamental Research Funds for the Central Universities under Grant 2682017CX046 and Grant A0920502052820-21, and in part by the Subtask of National Key Research and Development Program under Grant 2016YFB1200401-102F.

ABSTRACT Feature-based (FB) algorithms for automatic modulation recognition of radar signals have received much attention since they are usually simple to realize. However, existing FB approaches usually focus on several specific modulations and fail when applied to various modulations. To overcome this issue, we propose a simple and effective FB algorithm based on Manhattan distance-based features (MDBFs) in this paper. MDBFs are new features for radar signals that can be applied for recognition of different modulations. The main contributions of this paper are as follows. First, radar signals are represented as wavelet ridges, which includes important information that can distinguish different modulations, and the piecewise aggregate approximation algorithm is introduced to reduce signal dimensions. Then, the dynamic time warping averaging is employed instead of the traditional k-means algorithm to extract realistic centroids for each class. Finally, the Manhattan distances between each data sample and each centroid are used to construct MDBFs, and decisions are made using the k-nearest neighbor. In addition, we prove that MDBFs have better class separability power than the Euclidean-based features. MDBFs contain information about the correlations between different classes, which means that these features suitable for discriminating various modulations when their class distributions do not overlap badly in representation space. The extensive experiments on a synthetic dataset demonstrate the outstanding performance of our proposed method and are hardly affected by the pulse width of the signal. Thus, the proposed method with the effectiveness and robustness could be a promising modulation recognition method of the radar signal.

INDEX TERMS Modulation recognition, Manhattan distance-based feature, wavelet ridge, dynamic time warping averaging, class centroid.

I. INTRODUCTION

Modulation recognition is an important signal processing task in radar reconnaissance, and it can be divided into intentional modulation (IMOP) recognition and unintentional modulation (UMOP) [1] recognition. IMOP is designed for *ad hoc* objectives, such as reducing the probability of interception, and improving the capability of anti-jamming and detection [2]. In the early IMOP recognition studies, five parameters, including carrier frequency (CF), PW, pulse amplitude (PA), angle of arrival (AOA) and time of arrival (TOA), were used to identify the IMOP. However, with the increasing complexity of the electromagnetic environment, the recognition performance of the five parameters is insufficient for various kinds of complicated and hybrid IMOPs.

To improve IMOP recognition performance, more studies have begun focused on extracting the significant features of radar signals that can be used to make decisions; such methods are called feature-based (FB) methods. FB methods are simple to implement and achieve near-optimal performance when designed properly [3]. In order to make learning algorithms less dependent on feature engineering, learning good representations of data have become a hot issue in recent years, especially the methods using deep learning-based, such methods are called representation-based (RB) methods [4]. However, the recognition processing of deep learning-based methods is hardly to explain.

The associate editor coordinating the review of this manuscript and approving it for publication was Jafar A. Alzubi.

2169-3536 © 2019 IEEE. Translations and content mining are permitted for academic research only.
Personal use is also permitted, but republication/redistribution requires IEEE permission.
See http://www.ieee.org/publications_standards/publications/rights/index.html for more information.

In this research, we propose a novel FB approach for both basic modulations and complicated or hybrid modulations, for which hybrid recognition method based on Manhattan distance-based features (MDBFs) and k-NN is used. This method contains three parts: *radar signal representation*, *feature extraction* and *decision making*. In the first part, we reconstruct the radar signal as a wavelet ridge that represents the instantaneous frequency of the radar signals; and different modulations have different overall wavelet ridge shape. Consequently, extracting the wavelet ridge of a signal is widely used in modulation recognition problems. In the second part, MDBF, which is a novel distance-based feature that improves classification performance, is proposed. Similar to the classic method, we first need to obtain exact centroids that directly impact the recognition performance of the features. Thus, we use the DTW [5], [6] barycenter averaging (DBA) algorithm instead of the traditional k-means to obtain realistic centroids for each class. Subsequently, MDBFs are constructed by calculating the Manhattan distance between the data and each centroid. Distance-based features have been applied to many pattern classification problems, e.g., intrusion detection [7], speech detection [8], and hand geometry authentication [9].

Before extracting the MDBFs, we first use the singular value decomposition (SVD) [10] denoising algorithm to remove the impact of noise on the recognition performance. Then, to reduce the time cost, we reduce the dimensions of data using the PAA algorithm [11]. Finally, we normalize the data to eliminate the influence of amplitude. In the last part, MDBFs are used for recognition using k-NN. Simulation results show that our method achieves higher recognition accuracy than the two existing methods for the nine modulations, one classic FB method proposed in [2] and another distance-based feature proposed in [7].

The rest of this paper is organized as follows. Section 2 reviews the work related to modulation recognition. The proposed recognition method is briefly reviewed in Section 3. Section 4 presents a detailed description of how the radar signal is transformed into the wavelet ridge. MDBF extraction and time complexity are presented in Section 5. The simulation results and analysis are presented in Section 6, and Section 7 provides the conclusions.

II. RELATED WORK OF MODULATION RECOGNITION

A. FEATURE-BASED METHOD

Hybrid expert features and machine learning algorithms are valuable research subject in modulation recognition because they are easy to implement, and many methods have been proposed in the past few years. These methods mainly focus on extracting features that can effectively distinguish radar signals of several different modulations and then predict modulation types by using machine learning methods such as neural network (NN), support vector machine (SVM) or k-NN.

In this case, time-frequency analysis has attracted much attention since it details variations in frequency with time in a two-dimensional (2D) time-frequency space [1], [2], [10], [11]– [24]. For example, a recognition method based on short-time Fourier transform (STFT) with accuracies over 94% under a low signal-to-noise (SNR) for binary phase shift keying (BPSK), quadrature phase-shift keying (QPSK), frequency shift keying (FSK) and linear frequency modulation (LFM) was proposed in [14]. The main ridge slice feature of the ambiguity function (AF) was extracted in [22] and combined with the kernel fuzzy c-means (KFC) algorithm to achieve higher recognition accuracy than the classic method for six modulations. Seven-dimensional statistical features of wavelet ridge were extracted in [2], and high recognition accuracy was achieved for six basic modulations using an SVM classifier. A two-dimensional feature of the time-frequency-energy distribution was extracted for classification using the relevance vector machine (RVM) [24]. This method can recognize three modulations: LFM, BPSK and QPSK. The above features are directly extracted from the time-frequency distribution (TFD) series, and they describe instantaneous properties of the radar signal. Additionally, some of expert features, called image features, are obtained from the TFD image. For example, in [16] and [25], Choi-Williams time-frequency distribution (CWD) image processing was used to extract radar signal features and successfully recognition several modulations at low SNR. In [26], the signal features were extracted based on STFT image processing, and then a binary decision tree was exploited to obtain an accuracy over 90% at low SNR for four modulations. Note that image processing, including image binarization, image enhancement, and image opening operation, is crucial for image features extractions,

Nevertheless, most expert features that rely on the analysis of a mathematical model of the signal leads to fail when applied to various modulations because they focus on several specific modulations only. In this paper, we present a universal data-driven approach that learn features from an existing training dataset and is suitable for various modulations.

B. DEEP LEARNING-BASED METHOD

With the development of deep learning, an increasing number of deep learning methods have been used in modulation recognition. These methods are used to designed end-to-end models, including deep neural networks, such as convolutional neural network (CNN), the deep auto-encoder network (DAE), deep belief network (DBN) to auto-learn new features for data representations and make decisions These approaches can generally achieve better recognition accuracy than classic FB methods.

Converting radar signals to time-frequency representations as input of deep learning network is the most common method. For example, in [27] and [28], using TFD array as input of CNN to recognition different modulations. Similarly, the modulation identification could be regarded as an image recognition problem in which a deep learning network can

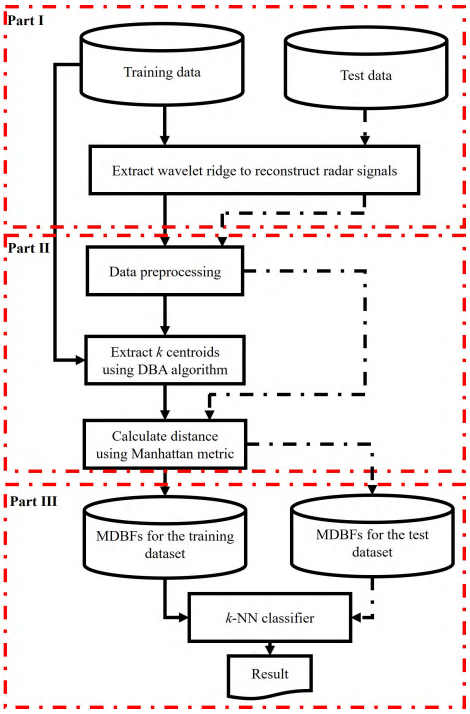

FIGURE 1. Framework of modulation recognition based on MDBF.

be trained using TFD images of radar signal [29]– [34]. Then, the test data would be predicted using the trained deep model. Additionally, deep learning networks were treated as classifier for prediction in [35] and [36], using several expert features including second order statistics features, entropy features, instantaneous features and five classical parameters. In fact, a procedure that treats a deep network as a classifier can be seen as a hybrid expert features and machine learning method.

Unfortunately, deep learnings are black box models that cannot explain exactly how the model works, and the features learned from deep neural networks are beyond human comprehension. In contrast, we explore interpretable features in our proposed method, and each feature denotes the correlation between different classes.

III. RECOGNITION FRAMEWORK OVERVIEWS

The automatic recognition of various modulations is studied in this paper. A hybrid recognition framework based on MDBFs and k-NN is proposed, as shown in **Fig. 1**. The framework can be divided into three parts, *radar signal representation*, *MDBFs extraction* and *modulation recognition using a k-NN classifier*. The second part is crucial, because the MDBF, which can provide valuable information for the k-NN classifier to help improve accuracy for various modulations, is extracted. The overall framework is described in detail as follows:

Part I. In this part, wavelet ridges are applied to reconstruct radar signals. Let dataset $\mathbf{D}_r$ which includes k disjoint classes, and $\mathbf{D}_e$ be the reconstructed training dataset and the test dataset, respectively.

Part II. Each wavelet ridge sample in $\mathbf{D}_r$ first undergoes data denoising to eliminate the influence of noise. Then each sample undergoes dimensionality reduction to reduce the time cost and keep the length of each sample consistent. Furthermore, considering that MDBFs includes structural information only, energy normalization is necessary to eliminate the effect of the amplitude. After the above preprocessing, k different centroids $\mathbf{D}_c = \{\mathbf{c}_1, \cdots, \mathbf{c}_k\}$ can be extracted from $\mathbf{D}_r$ using the DBA algorithm. Finally, we can obtain a k-dimensional MDBFs by computing the Manhattan distance between it and $\mathbf{c}_i$, where $i = 1, \cdots, k$.

Part III. To perform the recognition, $\mathbf{D}_r$ and $\mathbf{D}_e$ are first transformed into new datasets $\mathbf{D}_r^{'}$ and $\mathbf{D}_e^{'}$, respectively. Each sample in $\mathbf{D}_r^{'}$ and $\mathbf{D}_e^{'}$ is formed of k-dimensional MDBF. In the last, the decision results of $\mathbf{D}_e^{'}$ are achieved by the k-NN classifier based on the $\mathbf{D}_r^{'}$.

As we know, k-NN is a simple and effective classification algorithm, and has been applied in many practical classification tasks [37]– [40]. In this paper, the k-NN algorithm was chosen instead of the SVM which is widely used for three reasons. First, SVM have many parameters to tune, while k-NN have one parameter only and easy to implement [39], which makes our experiments easy to replicate. Second, SVM require a large dataset to maximum prediction accuracy, while k-NN require a relatively small [38]. Third, the performance of the 1-NN ($k = 1$) directly reflects the power of different features used [39]. In fact, MDBFs can obtain good performance with all classical classification algorithm. For comparison to classification power of features better and replicate experiments easy, the 1-NN classifier has been selected in our paper.

For **Part I** and **Part II**, there are three important issues that need to be addressed regarding the extraction of the wavelet ridge of the signal, the identification of the centroids of each class and the calculate the MDBFs. These issues will be addressed in the following sections.

IV. RADAR SIGNAL REPRESENTATION USING WAVELET RIDGE

In this section, we employ wavelet ridge to represent the radar signal because it can reflect the change of frequency in a 2D time-frequency space and because the structural information of the wavelet ridge differs for different modulations. Theoretical studies have illustrated that the wavelet ridge includes all information of the original radar signal [41], [42].

For a real radar signal $s(t)$, let its analytic signal be $Z_s(t)$, which can be calculated by

$$Z_s(t) = s(t) + iH[s(t)] = A(t)e^{i\varphi(t)} \tag{1}$$

where the function $H[s(t)]$ is the Hilbert transform of $s(t)$, and $s(t)$ can be written as

$$s(t) = A(t)\cos\varphi(t) \tag{2}$$

where $A(t)$ denotes the instantaneous amplitude. From Equation (1), the instantaneous frequency of signal $s(t)$ is

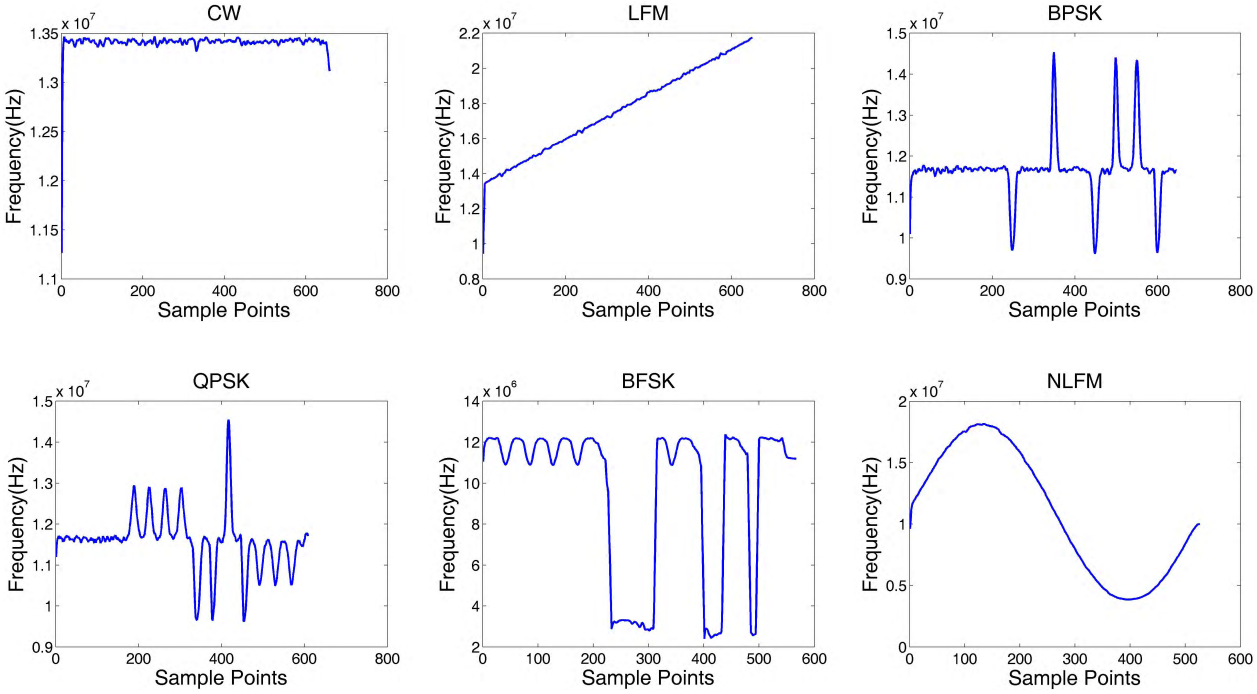

FIGURE 2. Examples of wavelet ridge curves for six different modulations, including a CW signal, an LFM signal, a BPSK signal, a QPSK signal, a BFSK signal and NLFM.

defined as

$$\omega(t) = \frac{1}{2\pi}\frac{d\varphi(t)}{dt} \tag{3}$$

Assuming that the analytic asymptotic wavelet is of the form $\psi(t) = A_\psi(t)e^{i\theta_\psi(t)}$, the wavelet transform (WT) of $s(t)$ can be calculated as

$$\begin{aligned} W_z(a,b,\psi) &= \langle s,\psi\rangle = \frac{1}{2}\langle Z_s,\psi\rangle \\ &= \frac{1}{2a}\int_{-\infty}^{\infty} A(t)A_\psi(\frac{t-b}{a})\cdot\exp(i\phi_{a,b}(t))dt \end{aligned} \tag{4}$$

where

$$\phi_{a,b}(t) = \varphi(t)\text{-}\theta_\psi(t-b/a) \tag{5}$$

According to the stationary phase theorem given in [41], Equations (4) can be approximated as

$$\begin{aligned} W_z(a,b,\psi) \approx \frac{1}{2a}&\frac{\sqrt{2\pi}\exp(i(\pi/4)\mathrm{sgn}(\phi''_{a,b}(t_s)))}{\sqrt{\left|\phi''_{a,b}(t_s)\right|}} \\ &\bullet A(t_0)A_\psi(\frac{t_s-b}{a})\exp(i\phi_{a,b}(t_s)) \end{aligned} \tag{6}$$

Letting the phase coefficients of $W_z(a,b,\psi)$ be

$$\Phi(a,b)=\arg[W_z(a,b,\psi)]=\frac{\pi}{4}\mathrm{sgn}[\phi''_{a,b}(t_s)]+\phi_{a,b}(t_s) \tag{7}$$

the derivative of $\Phi(a,b)$ with respect to b can be calculated as

$$\left.\frac{\partial\Phi(a,b)}{\partial b}\right|_{t_s=b} = \frac{\theta'_\psi(0)}{a} \tag{8}$$

The wavelet ridge is defined as $\mathbf{R} = \{(a_r,b)\,, t_s\,(a_r,b)=b\}$ and Equation (8) indicates that wavelet point a_r can be calculated by a simple iterating algorithm [42]. Here, we assume that the discrete sampled radar signal can be expressed as follows:

$$s(k) = s(kT_s), k=0,1,\cdots,N-1 \tag{9}$$

where T_s is the sampling cycle, and N is the number of sampling points. Let $\mathrm{D}_b(\Phi(a,b))$ be the discrete differential function of $\Phi(a,b)$ with respect to b, and $(a_r(kT_s),kT_s)$ is the ridge point with respect to kT_s. Thus, the extraction algorithm of the wavelet ridge is as follows:

Step 1. Let $a_0(kT_s)$ be the initial estimator of $a_r(kT_s)$.

Step 2. Calculate $a_{i+1}(kT_s)$ according to Equation (10), i.e., the value can be calculated by

$$a_{i+1}(kT_s) = \omega_0/\mathrm{D}_b(\Phi(a_i,kT_s)) \tag{10}$$

Step 3. Assuming that ξ is a small fixed positive value of the required precision, when $a_{i+1}(kT_s)$ satisfies

$$\left|(a_{i+1}(kT_s)-a_i(kT_s))/a_i(kT_s)\right| < \xi \tag{11}$$

the algorithm finds a ridge point, and consequently $a_r(kT_s)$ is equal to $a_{i+1}(kT_s)$. In addition, it is necessary to update the value of k to $k=k+1$.

Step 4. Repeat Step 2 and Step 3 until $k > N$-1; then, all ridges are connected to a wavelet ridge [41].

Fig. 2 shows an example of the six types of wavelet ridges of radar signals, including a wave pulse with constant frequency (CW), LFM, BPSK, QPSK, binary frequency-shift keying (BFSK) and nonlinear frequency

modulation (NLFM). The complex morlet wavelet has been selected as the mother wavelet for the WT, because its good time-frequency localization [42]. **Fig. 2** shows that different IMOPs have different wavelet ridge curve structures.

V. FEATURE EXTRACTION

The goal of this section is to extract the MDBFs. Compared to the traditional features extracted by analyzing the mathematical models of signals, our method is a data-driven approach that directly mines the valuable information in the dataset. Our method can classify for the IMOPs more accurately and is not limited to basic modulations. One of the reasons for this result is that, the traditional features are generally highly abstract and subtle information is ignored, while the MDBFs are extracted by calculating the distance between the data and each disjoint centroid and thus, includes global structural information. In this section, the MDBF extraction method will be introduced in detail. We use the Manhattan metric instead of the conventional Euclidean metric so that the MDBFs achieves better class separability power, we provide a simple proof in this section.

A. DATA PREPROCESSING

Three different pre-processing steps, i.e., *signal denoising*, *dimensionality reduction*and*energy normalization* will be considered before extracting MDBFs.

1) DATA DENOISING

Considering that received radar signal is inevitably affected by noise in a complex electromagnetic environment, the overall shape of the wavelet ridge will be seriously distorted when the SNR is too low. Thus, we employ the SVD denoising method to eliminate the influence of the noise components of the wavelet ridge in this paper.

2) DIMENSIONALITY REDUCTION

Employing dimensionality reduction approach can reduces the time cost require for feature calculation and results in consistent dimensions for each sample. Here, we employ the PAA algorithm for the dimensionality reduction, which is described as follows:

For a m-dimensional wavelet ridge $\mathbf{w}_m = \{x_1, \cdots, x_m\}$, let its N-dimensional vector after dimensionality reduction be $\mathbf{w}_N = \{y_1, \cdots, y_N\}$, The i th element of $\overline{\mathbf{w}}$ is calculated by the following equation:

$$y_i = \frac{N}{m} \sum_{j=\frac{m}{N}(i-1)+1}^{\frac{m}{N}i} x_j \tag{12}$$

Intuitively, $\mathbf{w}_m$ is first divided into N equal-sized "frames," and then, each mean value of the data that falls within each frame is calculated, and a new vector of these values becomes the reduced representation [11].

3) ENERGY NORMALIZATION

To eliminate the influence of the amplitude, energy normalization is used. For a wavelet ridge sample $\mathbf{w}_N=\{y_1, \cdots, y_N\}$, let its normalized vector be $\overline{\mathbf{w}}_N=\{\bar{y}_1, \cdots, \bar{y}_N\}$. Thus, the ith element of $\overline{\mathbf{w}}_N$ can be calculated as

$$\overline{y_i} = \frac{y_i}{\sqrt{\sum_{j=1}^{N} y_j^2}} \tag{13}$$

B. CENTROID EXTRACTION USING DBA

The k-means algorithm is generally used to identify centroids (averaging object) in many studies on distance-based feature extraction [7], [43] since it is easy to realize and its computational cost is low. However, k-means has two drawbacks. (i) The k-means algorithm computes the centroid of the clusters using Euclidean averaging, but Euclidean averaging may produce spurious objects that do not resemble any parent objects because Euclidean averaging is susceptible to the dislocation and displacement of data. (ii) The cluster of each iteration is not disjointed from each other clusters. To avoid these drawbacks, a global averaging approach under dynamic time warping is presented in [44] and [45] is used in our method. The method averages the sample for each class and is insensitive to warped data. DBA is considered the state-of-the-art method for extracting centroids, its algorithm has been described in detail in [44], and a proof of its convergence is presented in [45].

Fig. 3 shows an example to compare the performance of DBA with that of Euclidean averaging. **Fig. 3 (a)** shows three different probability density functions (PDFs) of normal distribution. When averaged with Euclidean averaging, the result exhibits a spurious peak that does not exist in arbitrary parent objects (shown in **Fig. 3 (b)**), while the results from the DBA algorithm is resemble to the parent objects (shown in **Fig. 3 (c)**).

C. DEFINITION OF MDBF AND EXTRACTION METHOD

After the centroid of each class has been identified, the distances between the data and each centroid can be calculated. The Euclidean and Manhattan distance metrics are widely used because of their simplicity and effectiveness. For two data samples $\mathbf{Q} = \{q_1, \cdots, q_n\}$ and $\mathbf{P} = \{p_1, \cdots, p_n\}$, the Euclidean distance is obtained as

$$\mathrm{ED}(\mathbf{Q}, \mathbf{P}) = \sqrt{\sum_{i=1}^{n} (q_i - p_i)^2} \tag{14}$$

The Manhattan distance is defined as

$$\mathrm{MD}(\mathbf{Q}, \mathbf{P}) = \sum_{i=1}^{n} |q_i - p_i| \tag{15}$$

In this paper, the Manhattan distance is used for the reason that explained in Section 4.4. Because we apply the PAA algorithm to reduce dimensionality during the preprocessing, Equation (15) will be rewritten to guarantee that there are no false dismissals [11]. Suppose an n-dimensional data sample $\mathbf{Q}$ is reduced to an N-dimensional sample $\overline{\mathbf{Q}} = \left\{\overline{q}_1, \cdots, \overline{q_N}\right\}$. Then, the

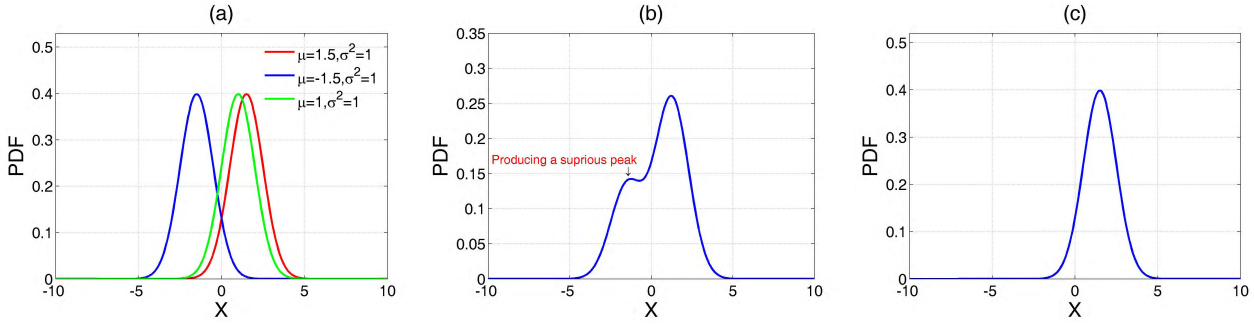

FIGURE 3. Examples of extracting a centroid using the DBA algorithm and Euclidean averaging: (a) three types of normal distribution curves with different means (μ) and standard deviations (σ); (b) extracting centroid using Euclidean averaging; and (c) extracting a centroid using the DBA algorithm.

Manhattan distance between $\overline{\mathbf{Q}}$ and another data sample $\bar{P} = \{\bar{p}_1, \cdots, \bar{p}_N\}$ can be calculated as

$$\overline{\mathrm{MD}}\left(\overline{\mathbf{Q}}, \overline{\mathbf{P}}\right) = \sum_{i=1}^{N} |\overline{q}_i - \overline{p}_i| * \sqrt{\frac{n}{N}} \tag{16}$$

We will use Equation (16) to calculate the distance between the data sample and each centroid. Assume k different centroids $\mathbf{D}_c = \{\mathbf{c}_1, \cdots, \mathbf{c}_k\}$ have been identified, where $\mathbf{c}_i$ $(i = 1, \cdots, k)$ is an N-dimensional vector. Therefore, the k-dimensional MDBFs of $\overline{\mathbf{Q}}$ can be calculated. The ith MDBF feature value of $\overline{\mathbf{Q}}$ is defined as

$$\mathrm{MDBF}\,(i) = \overline{\mathrm{MD}}\left(\bar{Q}, \mathbf{c}_i\right), i = 1, \cdots, k \tag{17}$$

For an arbitrary n-dimensional data sample, assume that k disjoint centroids have been identified; then, its k-dimensional MDBFs extraction procedure can be described in three steps:

Step 1. Transform the radar signal to the wavelet ridge.

Step 2. Preprocess the wavelet ridge sample using the SVD denoising method, the PAA algorithm and energy normalization.

Step 3. Calculate the Manhattan distance between the wavelet ridge sample and each centroid; a k-dimensional vector of these distance values becomes the sample representation.

D. WHY NOT EUCLIDEAN METRIC?

We want to explain the reason for choosing the Manhattan metric instead of the Euclidean metric. For convenience, we analyze a binary classification problem, but the conclusion can be easily extended to multi-class problems. Assuming that $\mathbf{D}_1$ and $\mathbf{D}_2$ are two disjoint datasets, their centroids are $\mathbf{c}_1$ and $\mathbf{c}_2$, respectively (shown in **Fig. 4**). For data sample $\mathbf{x} \in \mathbf{D}_1$, its distance-based feature vector can be expressed as

$$\mathbf{x} = [\mathrm{dist}(\mathbf{x}, \mathbf{c}_1), \mathrm{dist}(\mathbf{x}, \mathbf{c}_2)] \tag{18}$$

where dist(•) represents a distance metric. Intuitively, the larger the value of $|\mathrm{dist}(\mathbf{x}, \mathbf{c}_1) - \mathrm{dist}(\mathbf{x}, \mathbf{c}_2)|$, the better the class separability power. Therefore, we need to prove that Equation (19) is established.

$$\mathrm{MD}(\mathbf{x}, \mathbf{c}_2) - \mathrm{MD}(\mathbf{x}, \mathbf{c}_1) > \mathrm{ED}(\mathbf{x}, \mathbf{c}_2) - \mathrm{ED}(\mathbf{x}, \mathbf{c}_1) \tag{19}$$

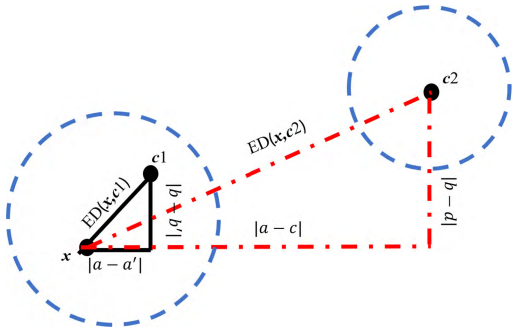

FIGURE 4. Distribution of centroids $\mathbf{c}_1$, $\mathbf{c}_2$, and sample x.

For convenience, we analyze in 2D space. Assuming that $\mathbf{x} = [a, b]^{\mathrm{T}}$, $\mathbf{c}_1 = [a', b']^{\mathrm{T}}$, and $\mathbf{c}_2 = [c, d]^{\mathrm{T}}$, where $c > a' > a$, $d > b' > b$, and their relation of space is shown in **Fig. 4**, let $\Delta 1$ be $\mathrm{ED}(\mathbf{x}, \mathbf{c}_2) - \mathrm{ED}(\mathbf{x}, \mathbf{c}_1)$, which can be calculated as follows:

$$\begin{aligned}\Delta 1 &= \sqrt{(a-c)^2 + (b-d)^2} - \sqrt{\left(a-a'\right)^2 + \left(b-b'\right)^2} \\ &= \frac{(a-c)^2 + (b-d)^2 - \left(a-a'\right)^2 - \left(b-b'\right)^2}{\mathrm{ED}(\mathbf{x}, \mathbf{c}_2) + \mathrm{ED}(\mathbf{x}, \mathbf{c}_1)} \\ &= \frac{\left(c-a'\right)\left(c-2a+a'\right) + \left(d-b'\right)\left(d-2b+b'\right)}{\mathrm{ED}(\mathbf{x}, \mathbf{c}_2) + \mathrm{ED}(\mathbf{x}, \mathbf{c}_1)}\end{aligned} \tag{20}$$

Let $\Delta 2$ be $\mathrm{MD}(\mathbf{x}, \mathbf{c}_2) - \mathrm{MD}(\mathbf{x}, \mathbf{c}_1)$ so that $\Delta 2$ can be calculated as:

$$\begin{aligned}\Delta 2 &= |a-c| + |b-d| - \left|a-a'\right| - \left|b-b'\right| \\ &= \left(c-a'\right) + \left(d-b'\right)\end{aligned} \tag{21}$$

because

$$\begin{aligned}\left(c-2a+a'\right) &= (c-a) + \left(a'-a\right) \\ &< \mathrm{ED}(\mathbf{x}, \mathbf{c}_2) + \mathrm{ED}(\mathbf{x}, \mathbf{c}_1)\end{aligned} \tag{22}$$

Similarly

$$\left(d-2b+b'\right) < \mathrm{ED}(\mathbf{x}, \mathbf{c}_2) + \mathrm{ED}(\mathbf{x}, \mathbf{c}_1) \tag{23}$$

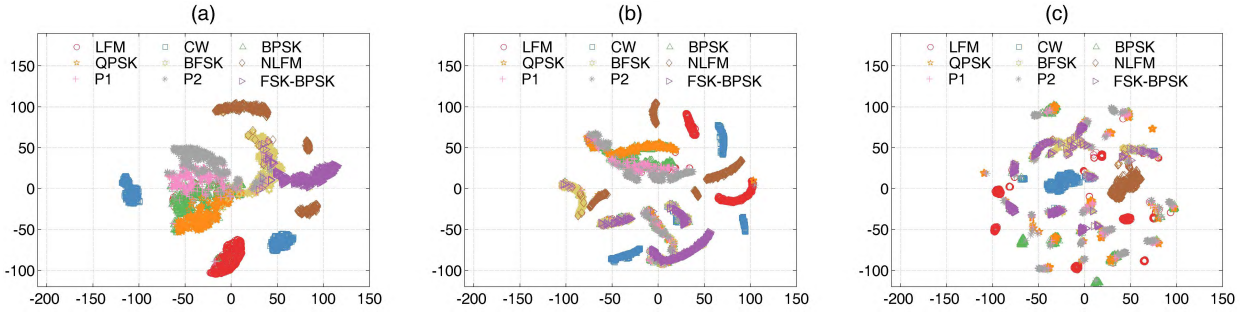

FIGURE 5. T-sne visualization of classes in 2D space. (a) Distribution of the MDBFs (b) Distribution of the DSFs (c) Distribution of the WRFCCFs.

Thus, the inequality $\Delta 1 < \Delta 2$ is true, and Equation (19) is established. The conclusion is also true for multiclass problems.

E. COMPUTATIONAL COMPLEXITY ANALYSIS

The aim of this section is to evaluate the time complexity of extracting the MDBF in detail. Here, we analyze the time complexity of each part, and then sum them as the total time complexity.

An arbitrary n-dimensional wavelet ridge can be calculated using a simple iterative search algorithm, which is described in Section 2, with its time complexity is $\Theta(I_0 \cdot n^2 \cdot \log(n))$, where I_0 is the number of iterations and n is the length of the radar signal. After extracting the wavelet ridge, we employ three preprocessing methods on the wavelet ridge: the elimination of the influence of noise using SVD denoising, which has a time complexity of $\Theta(n^2)$, dimensionality reduction using PAA which has a time complexity of $\Theta(m)$, where m denotes the reduced dimension, and normalization with respect to energy, which has a linear time complexity of $\Theta(m)$. For the existing M-dimensional training data, the time complexity of the DBA algorithm is $\Theta(I \cdot M \cdot m^2)$ [43], where the parameter I denotes the number of iterations. Obviously, when large training datasets or long signal lengths appear, time complexity will increase rapidly. Finally, the calculation of k Manhattan distances have linear complexity $\Theta(k \cdot m)$.

In fact, the wavelet ridge extraction process converges fast [41], and the centroids can be calculated offline; thus, the overall time complexity of extracting a MDBF is

$$\begin{aligned}\Theta(\mathrm{DFMM}) &= \Theta\left(I_0 \cdot n^2 \cdot \log(n) + n^2 + 2m + k \cdot m\right) \\ &= \Theta\left(I_0 \cdot n^2 \cdot \log(n)\right) \end{aligned} \tag{24}$$

VI. SIMULATION AND RESULTS ANALYSIS

A. DATA DESCRIPTION

To evaluate the recognition performance of the proposed approach, we simulate nine modulations: CW, LFM, BPSK, QPSK, BFSK, NLFM, multi–discrete phase coded (MDPC) and frequency shift keying-binary phase shift keying (FSK-BPSK); their modulation parameters are shown in **Table 1**. To improve the credibility of the simulation, we set the root mean square error (RMSE) for CF and PW to be 1 MHz and 1 μs, respectively.

TABLE 1. Parameters for IMOP of radar signals.

Parameters	Values
Sampling frequency	60 MHz
Carrier frequency	10~15 MHz
Pulse width	10 μs
Bandwidth of LFM	7 MHz
13-bit Barker codes for BPSK	[1, 1, 1, 1, 1, 0, 0, 1, 1, 0, 1, 0, 1]
16-bit Frank codes for QPSK	[0, 0, 0, 0, 0, j, 1, −j, 0, 1, 0, 1, 0, −j, 1, j,]
Code for BFSK	[1, 1, 1, 1, 1, 0, 0, 1, 1, 0, 1, 0, 1]
Code for MDPC	P1 code and P2 code
Two frequency points for BFSK	[2 MHz, 10 MHz]
Sine curve for NLFM	/
SNR of the test data	[0, 3, 6, 9, 12] dB
SNR of the training data	10~15 dB
RMSE of the CF and PW	1 MHz and 1 us

According to the parameter information, each modulation simulates twenty samples at SNR values of 10∼15 dB to train classifier. Each modulation generates one hundred samples at SNR values of [0, 3, 6, 9, 12] dB. Thus, a total of 900 samples are generated at each SNR to test performance. Note that the simulations that follow were completed in the MATLAB environment.

B. PERFORMANCE METRIC

Considering the number of each class is identical, the correct recognition rate (CRR) is applied to assess the discriminative performance. CRR can be calculated by

$$\mathrm{CRR} = \frac{\text{correct recognition samples}}{\text{all samples}} \times 100\% \tag{25}$$

C. RECOGNITION PERFORMANCE

We design a simulation to verify the performance of our method compared to the two existing methods: the distance sum-based feature (DSF) method from [7] and the traditional feature method from [2]. Each element of DSF is the sum of the distances between the sample and centroids. The traditional feature is a seven-dimensional statistical feature of the

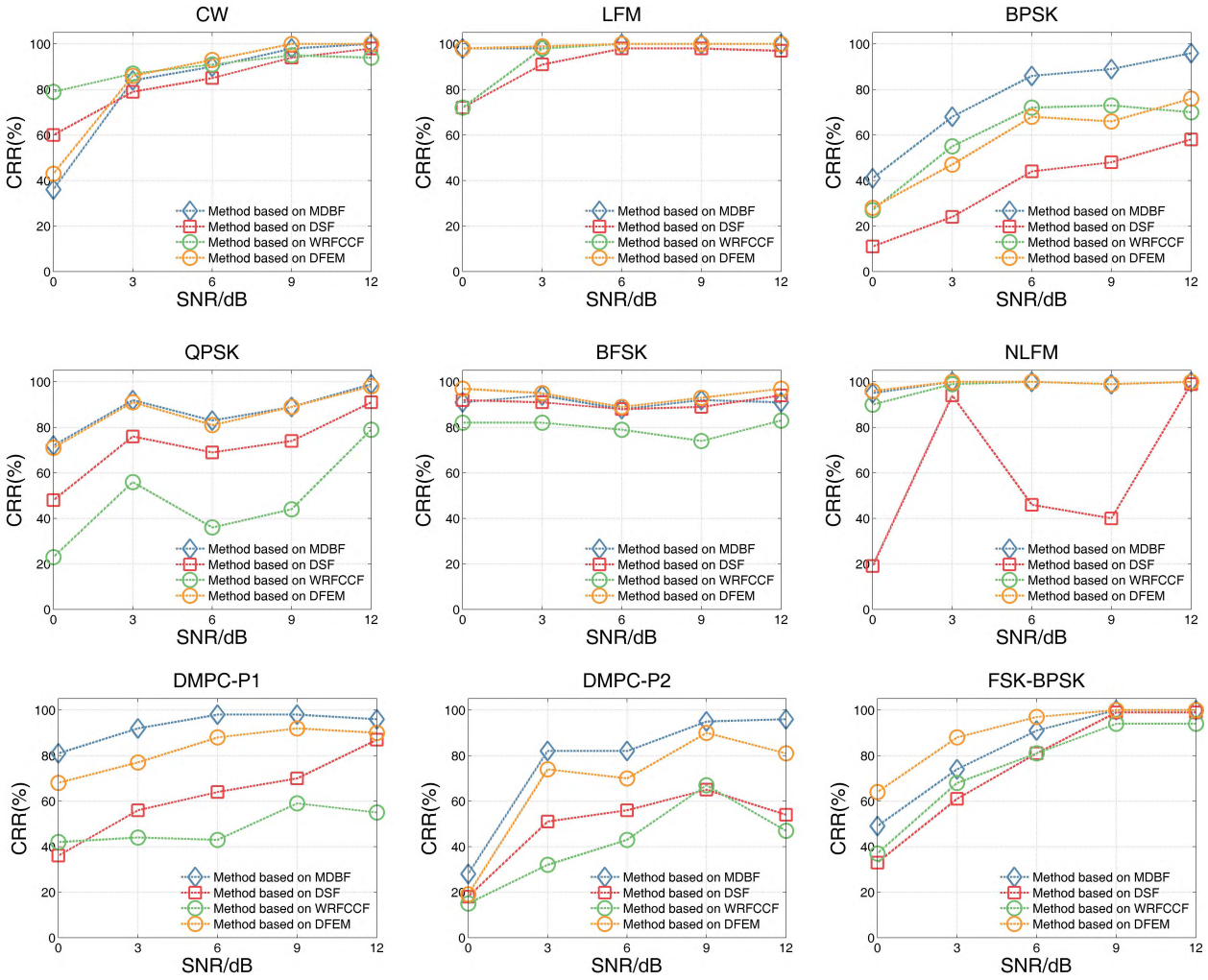

FIGURE 6. CRR versus different SNR values for different methods, including LFM, BPSK, QPSK, BFSK, NLFM, MDPC-P1, MDPC-P2, and FSK-BPSK.

wavelet ridge, which is called the wavelet ridge frequency cascade-connection feature (WRFCCF).

Before checking the recognition performance, we first show the disjoint class distribution in 2D feature space. For test data at SNRs of [0, 3, 6, 9, 12] dB in Section 5.1, DSF, MDBF and WRFCCF are multi-dimensional vectors, thus, we apply the t-distributed stochastic neighbor embedding (t-SNE) algorithm [46] to visualize them in **Fig. 5**. The parameters of the PAA algorithm and k-means are given in **Table 2**. In generally, the class distribution has a smaller intra-class compactness, and large inter-class scatter degree can make the features more discriminative. From the scatter plots shown in **Fig. 5a**, **5b** and **5c**, we can see that the class distributions based on the MDBFs and DSFs have lower intra-class compactness than do the WRFCCFs and a better inter-class scatter degree. Meanwhile, the overlap of the distribution with DSFs is greater than that of MDBFs, i.e., BPSK, QPSK, BFSK and MDPC are not resolved in **Fig. 5b**. Thus, the class separability of MDBFs is better than those of DSFs and WRFCCFs. Note that the dimensions in **Fig. 5** have no physical meaning and only numeric meaning.

TABLE 2. Parameter settings for the algorithms used in this paper. Let η be the dimension of the transformed space we wish to reduce.

Parameters	Values
Dimensional η for the PAA algorithm	300
k nearest neighbors for the k-NN classifier	1
k clusters for k-means	9

Here, we apply the k-NN classifier to obtain recognition results, and the parameter of the classifier is given in **Table 2**. To validate the performance of MDBFs, the distance features based on the Euclidean metric (DFEM) with the DBA algorithm were added into the experiment. CRR curves of nine modulations at SNRs of [0, 3, 6, 9, 12] dB are shown in **Fig. 6**. We can clearly see that the CRR of the four methods improves with increasing SNR, and our method outperforms DSF-based and WRFCCF-based methods in terms of CRR on the simulation data and better than the DFEM-based method (excluding for the FSK-BPSK signal). When SNR $=$ 3 dB, the proposed method achieves more than 90% recognition accuracy for CW, LFM, BFSK, NLFM and P1, and the

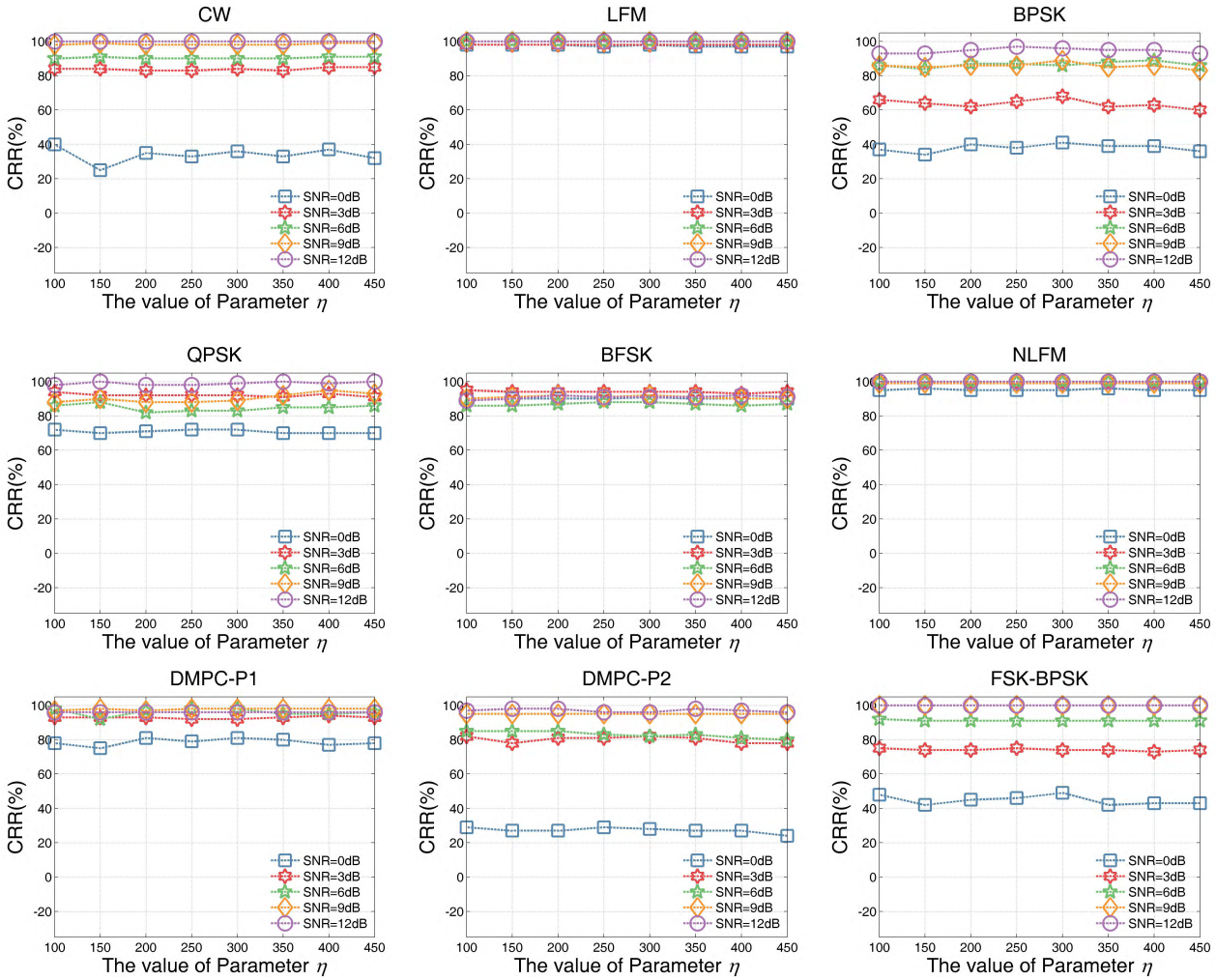

FIGURE 7. CRR versus η, including LFM signal, BPSK signal, QPSK signal, BFSK signal, NLFM signal, MDPC-P1 signal, MDPC-P2 signal, and FSK-BPSK signal.

accuracy is above 90% when SNR = 9 dB, except for the BPSK signal. For complicated and hybrid modulations (P1, P2 and FSK-BPSK), our method obtains more than 90% accuracy for SNR = 9 dB, while the other methods obtain low accuracy, especially for the P1 and P2 signals. Consequently, we can conclude that the proposed method performs better than the compared method.

D. ANALYZING PARAMETER SENSITIVITY

In this section, the effect of the parameter η of the PAA algorithm on the recognition accuracy will be analyzed. Let η be 100, 150, 200, 250, 300, 350, 400, and 450, and the other parameters are selected according to **Table 1**. **Fig. 7** shows the CRR versus η for nine different modulations.

Intuitively, the CRR of the nine modulations is stable under different SNRs. For example, the parameter η hardly affects the CRR of LFM, CW, NLFM and FSK-BPSK when SNR $>$ 3 dB, and has a slight effect for other modulations. We can give the following explanation: the PAA algorithm regards the mean value of the data in the ''frame'' as a representation of the data in the whole ''frame'' [11]; when the signal changes a small amount in a short time, the PAA algorithm can retain most of the information of the signal, conversely may lose some information. From **Fig. 2**, we can see that the wavelet ridge of LFM, CW and NLFM is a smooth curve. The curve does not change in a short time, while the wavelet ridges of the other modulations have subtle features that are most likely removed when using the PAA algorithm.

However, the overall effect of parameter η on recognition performance can be ignored, and the property means that our method is suitable for radar signals with arbitrary feature dimensions and without need to tun the parameter η to achieve an better result.

E. ANALYZING THE IMPACT OF THE PW

In the above experiments, the PW of the signal is fixed as 1 μs. However, PW is an important modulation parameter for the radar signal, and the radar signal received includes different PWs in a real environment. The conventional distance-base features do not carry the information of signal size

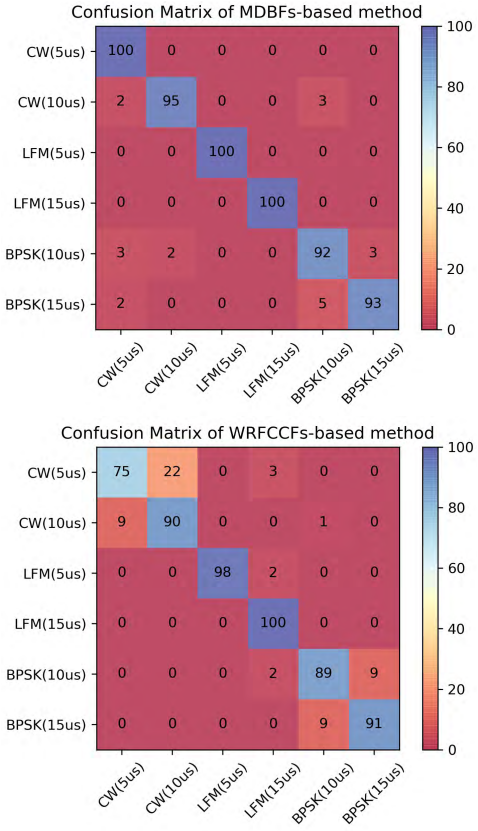

FIGURE 8. Confusion matrix for CW, LFM, and BPSK with different PWs when SNR = 12 dB.

(PW for the radar signal), although they are well applied to intrusion detection and speech detection. Different from the traditional distance-based features, the MDBFs are defined with the information of signal size and can identify modulations with different PWs in theory. In this section, the impact of the PWs of CW, LFM, and BPSK is discussed for MDBFs and WRFCCFs.

Each modulation simulates twenty samples to train the k-NN classifier at SNR values between 10 dB and 15 dB, and one hundred samples under SNR = 12 dB for testing. Let PW be 5 μs, 10 μs, 15 μs, and other parameters are set as listed in **Table 1**.

The confusion matrix for CW, LFM, and BPSK when SNR = 12 dB is shown in **Fig 8**. As suggested by the figure, MDBF-based method can discriminate modulations with different PWs very well, while WRFCCF-based method have difficulty discriminating the CW with different PWs. MDBF-based method can completely identify the LFM signal, yet on the CW signal and BPSK signals, it shows some inaccuracy, primarily because the shape of the wavelet ridge is distorted by noise.

VII. CONCLUSION

In this paper, a distance-based feature based on the Manhattan distance and the k-NN classifier for IMOP recognition is presented. In our method, modulated signals are first reconstructed as wavelet ridges. Subsequently, three methods, i.e., SVD denoising, the PAA algorithm and energy normalization, are applied to preprocess the data. Finally, the centroids are calculated for each class and MDBFs are extracted. MDBFs are calculated as by the Manhattan distance between the sample and each centroid. Although time complexity is high in the case of large training datasets or long signal lengths, our method can achieve higher accuracy than the two existing methods. The second simulation shows that our method has robust recognition performance over a wide range of values for parameter η for the PAA algorithm. Moreover, the ability of the MDBFs to separate modulations with different PWs is validated though the last experiment. However, the proposed method is realized based on some known patterns, and future work will focus on applying the technique to an unknown modulated signal.

REFERENCES

[1] P. Wang, Z. Qiu, J. Zhu, and B. Tang, "Autonomous radar pulse modulation classification using modulation components analysis," *EURASIP J. Adv. Signal Process.*, vol. 2016, p. 98, Sep. 2016.
[2] Z. B. Yu, "Research on radar emitter signal recognition based on intra-pulse features," Ph.D. dissertation, Southwest Jiaotong Univ., Chengdu, China, 2010.
[3] O. A. Dobre, A. Abdi, Y. Bar-Ness, and W. Su, "Survey of automatic modulation classification techniques: Classical approaches and new trends," *IET Commun.*, vol. 1, no. 2, pp. 137–156, Apr. 2007.
[4] J. Gou, L. Wang, Z. Yi, J. Lv, Q. Mao, and Y.-H. Yuan, "A new discriminative collaborative neighbor representation method for robust face recognition," *IEEE Access*, vol. 6, pp. 74713–74727, Dec. 2018.
[5] Z. Zhang, R. Tavenard, A. Bailly, X. Tang, P. Tang, and T. Corpetti, "Dynamic time warping under limited warping path length," *Inf. Sci.*, vol. 393, pp. 91–107, Jul. 2017.
[6] Y. Wan, X. L. Chen, and Y. Shi, "Adaptive cost dynamic time warping distance in time series analysis for classification," *J. Comput. Appl. Math.*, vol. 319, pp. 514–520, Aug. 2017.
[7] C. Guo, Y. Zhou, Y. Ping, Z. Zhang, G. Liu, and Y. Yang, "A distance sum-based hybrid method for intrusion detection," *Appl. Intell.*, vol. 40, no. 1, pp. 178–188, Jan. 2014.
[8] H. Takçı and T. Güngör, "A high performance centroid-based classification approach for language identification," *Pattern Recognit. Lett.*, vol. 33, no. 16, pp. 2077–2084, Dec. 2012.
[9] J. Burgues, J. Fierrez, D. Ramos, and J. Ortega-Garcia, "Comparison of distance-based features for hand geometry authentication," in *Proc. Eur. Workshop Biometrics Identity Manage.*, Berlin, Germany, 2009, pp. 325–332.
[10] X. Zhang, J. Wan, and Y. Zhao, "Recognition of radar emitter signals based on SVD and AF main ridge slice," *J. Commun. Netw.*, vol. 17, no. 5, pp. 491–498, Nov. 2015.
[11] E. Keogh, K. Chakrabarti, M. Pazzani, and S. Mehrotra, "Dimensionality reduction for fast similarity search in large time series databases," *Knowl. Inf. Syst.*, vol. 3, no. 3, pp. 263–286, 2001.
[12] T. R. Kishore and K. D. Rao, "Automatic intrapulse modulation classification of advanced LPI radar waveforms," *IEEE Trans. Aerosp. Electron. Syst.*, vol. 53, no. 2, pp. 901–914, Apr. 2017.
[13] J. Li, G. Zhang, Y. Sun, E. Yang, L. Qiu, and W. Ma, "Automatic intra-pulse modulation recognition using support vector machines and genetic algorithm," in *Proc. IEEE 3rd Inf. Technol. Mechatronics Eng. Conf. (ITOEC)*, Chongqing, China, Oct. 2017, pp. 309–312.
[14] F. Wang, S. Huang, H. Wang, and C. Yang, "Automatic modulation classification exploiting hybrid machine learning network," *Math. Problems Eng.*, vol. 2018, Dec. 2018, Art. no. 6152010.
[15] X. Zeng, "Automatic modulation classification of radar signals using the pseudo Margenau-Hill distribution," in *Proc. 10th Int. Conf. Comput. Autom. Eng.*, Brisbane, QLD, Australia, 2018, pp. 120–123.
[16] M. Zhang, L. Liu, and M. Diao, "LPI radar waveform recognition based on time-frequency distribution," *Sensors*, vol. 16, no. 10, pp. 1682–1702, Oct. 2016.

[17] X. Ma, D. Liu, and Y. Shan, "Intra-pulse modulation recognition using short-time ramanujan Fourier transform spectrogram," *EURASIP J. Adv. Signal Process.*, vol. 2017, p. 42, Dec. 2017.
[18] Q. Guo, P. Nan, and J. Wan, "Radar signal recognition based on ambiguity function features and cloud model similarity," in *Proc. IEEE 8th Int. Conf. Ultrawideband Ultrashort Impulse Signals (UWBUSIS)*, Odessa, Ukraine, Sep. 2016, pp. 128–134.
[19] Z. Zhang *et al.*, "Modulation signal recognition based on information entropy and ensemble learning," *Entropy*, vol. 20, no. 3, pp. 198–216, Mar. 2018.
[20] K. Konopko, Y. P. Grishin, and D. Jańczak, "Radar signal recognition based on time-frequency representations and multidimensional probability density function estimator," in *Proc. IEEE Signal Process. Symp. (SPSympo)*, Debe, Poland, Jun. 2015, pp. 1–6.
[21] J. Xie, "Robust intra-pulse modulation recognition via sparse representation," in *Proc. IEEE CIE Int. Conf. Radar (RADAR)*, Guangzhou, China, Oct. 2016, pp. 1–4.
[22] D. Zeng, H. Xiong, J. Wang, and B. Tang, "An approach to intra-pulse modulation recognition based on the ambiguity function," *Circuits, Syst. Signal Process.*, vol. 29, no. 6, pp. 1103–1122, Dec. 2010.
[23] J. Lunden and V. Koivunen, "Automatic radar waveform recognition," *IEEE J. Sel. Topics Signal Process.*, vol. 1, no. 1, pp. 124–136, Jun. 2007.
[24] Z. Yang, W. Qiu, H. Sun, and A. Nallanathan, "Robust radar emitter recognition based on the three-dimensional distribution feature and transfer learning," *Sensors*, vol. 16, no. 3, p. 289, Feb. 2016.
[25] E. R. Zilberman and P. E. Pace, "Autonomous time-frequency morphological feature extraction algorithm for LPI radar modulation classification," in *Proc. IEEE Int. Conf. Image Process.*, Atlanta, GA, USA, Oct. 2006, pp. 2321–2324.
[26] S. Liu, X. Yan, P. Li, X. Hao, and K. Wang, "Radar emitter recognition based on SIFT position and scale features," *IEEE Trans. Circuits Syst. II, Exp. Briefs*, vol. 65, no. 12, pp. 2062–2066, Dec. 2018.
[27] X. Wang, G. Huang, Z. Zhou, and J. Gao, "Radar emitter recognition based on the short time Fourier transform and convolutional neural networks," in *Proc. IEEE 10th Int. Congr. Image Signal Process., Biomed. Eng. Inform. (CISP-BMEI)*, Shanghai, China, Oct. 2017, pp. 1–5.
[28] T. J. O'Shea, J. Corgan, and T. C. Clancy, "Convolutional radio modulation recognition networks," in *Proc. Int. Conf. Eng. Appl. Neural Netw.*, Aberdeen, U.K., 2016, pp. 213–226.
[29] Q. Zhang, Z. Xu, and P. Zhang, "Modulation recognition using wavelet-assisted convolutional neural network," in *Proc. IEEE Int. Conf. Adv. Technol. Commun. (ATC)*, Ho Chi Minh City, Vietnam, Oct. 2018, pp. 100–104.
[30] Z. Zhou, G. Huang, H. Chen, and J. Gao, "Automatic radar waveform recognition based on deep convolutional denoising auto-encoders," *Circuits, Syst., Signal Process.*, vol. 37, no. 9, pp. 4034–4048, Jan. 2018.
[31] G. J. Mendis, J. Wei, and A. Madanayake, "Deep learning-based automated modulation classification for cognitive radio," in *Proc. IEEE Int. Conf. Commun. Syst. (ICCS)*, Shenzhen, China, Dec. 2016, pp. 1–6.
[32] F. Ç. Akyön, Y. K. Alp, G. Gök, and O. Arıkan, "Deep learning in electronic warfare systems: Automatic intra-pulse modulation recognition," in *Proc. IEEE 26th Signal Process. Commun. Appl. Conf. (SIU)*, Izmir, Turkey, May 2018, pp. 1–4.
[33] C. Wang, J. Wang, and X. Zhang, "Automatic radar waveform recognition based on time-frequency analysis and convolutional neural network," in *Proc. IEEE Int. Conf. Acoust., Speech Signal Process. (ICASSP)*, New Orleans, LA, USA, Mar. 2017, pp. 2437–2441.
[34] W. Ye and C. Peng, "Recognition algorithm of emitter signals based on PCA+CNN," in *Proc. IEEE 3rd Adv. Inf. Technol., Electron. Autom. Control Conf. (IAEAC)*, Chongqing, China, Oct. 2018, pp. 2410–2414.
[35] M. D. Ming Zhang and L. Guo, "Convolutional neural networks for automatic cognitive radio waveform recognition," *IEEE Access*, vol. 5, pp. 11074–11082, 2017.
[36] R. Cao, J. Cao, J.-P. Mei, C. Yin, and X. Huang, "Radar emitter identification with bispectrum and hierarchical extreme learning machine," *Multimedia Tools Appl.*, vol. 2018, pp. 1–18, May 2018.
[37] J. Gou, H. Ma, W. Ou, S. Zeng, Y. Rao, and H. Yang, "A generalized mean distance-based k-nearest neighbor classifier," *Expert Syst. Appl.*, vol. 115, pp. 356–372, Jan. 2019.
[38] S. B. Kotsiantis, "Supervised machine learning: A review of classification techniques," *Informatica*, vol. 31, no. 1, pp. 249–268, 2007.
[39] X. Wang, A. Mueen, H. Ding, G. Trajcevski, P. Scheuermann, and E. Keogh, "Experimental comparison of representation methods and distance measures for time series data," *Data Mining Knowl. Discovery*, vol. 26, no. 2, pp. 275–309, 2013.
[40] M. W. Aslam, Z. Zhu, and A. K. Nandi, "Automatic modulation classification using combination of genetic programming and KNN," *IEEE Trans. Wireless Commun.*, vol. 11, no. 8, pp. 2742–2750, Aug. 2012.
[41] N. Ozkurt and F. A. Savaci, "Determination of wavelet ridges of nonstationary signals by singular value decomposition," *IEEE Trans. Circuits Syst. II, Exp. Briefs*, vol. 52, no. 8, pp. 480–485, Aug. 2005.
[42] S. Li, X. Su, and W. Chen, "Wavelet ridge techniques in optical fringe pattern analysis," *J. Opt. Soc. Amer. A, Opt. Image Sci.*, vol. 27, no. 6, pp. 1245–1254, Jun. 2010.
[43] C.-F. Tsai, W.-Y. Lin, Z.-F. Hong, and C.-Y. Hsieh, "Distance-based features in pattern classification," *EURASIP J. Adv. Signal Process.*, vol. 2011, p. 62, Sep. 2011.
[44] F. Petitjean, A. Ketterlin, and P. Gançarski, "A global averaging method for dynamic time warping, with applications to clustering," *Pattern Recognit.*, vol. 44, no. 3, pp. 678–693, Mar. 2011.
[45] F. Petitjean, G. Forestier, G. I. Webb, A. E. Nicholson, Y. Chen, and E. Keogh, "Dynamic time warping averaging of time series allows faster and more accurate classification," in *Proc. IEEE Int. Conf. Data Mining*, Shenzhen, China, Dec. 2014, pp. 470–479.
[46] L. van der Maaten and G. Hinton, "Visualizing data using t-SNE," *J. Mach. Learn. Res.*, vol. 9, pp. 2579–2605, Nov. 2008.

YINGKUN HUANG received the B.S. degree in computer science and technology from Southwest University, Chongqing, China, in 2011, and the M.S. degree in electric engineering from Huaqiao University, Xiamen, China, in 2015. He is currently pursuing the Ph.D. degree with the Electrical Engineering Department, Southwest Jiaotong University, Chengdu, China. His research interests include machine learning, data mining, and knowledge discovery.

WEIDONG JIN was born in Anhui, China, in 1959. He received the B.S., M.S., and Ph.D. degrees from Southwest Jiaotong University, Chengdu, China, in 1982, 1989, and 1998, respectively. He has authored or co-authored more than 200 journal papers. His research interests include intelligent information processing and pattern recognition.

BING LI received the B.S. and M.S. degrees in electronic information science and technology and radio physics from the University of Electronic Science and Technology of China, Chengdu, in 2010 and 2013 respectively, and the Ph.D. degree in information and communication engineering from the South China University of Technology, Guangzhou, in 2016. She is currently a Lecturer with the School of Electrical Engineering, Southwest Jiaotong University. Her research interests include the time reversal method, imaging method, damage detection, wireless power transmission, and antennas and radio technology.

PENG GE received the B.E. degree in Jiangnan University, in 2008, and the Ph.D. degree from the University of Electronic Science and Technology of China, in 2017. From 2013 to 2014, he was a Visiting Scholar with the University of Naples, Italy, studying adaptive radar waveform design algorithms. His research interests include radar signal processing and analysis, radar waveform design, and machine learning.

YUNPU WU received the B.S. degree in electric engineering from Central South University, Changsha, China, in 2012. He is currently pursuing the Ph.D. degree with the Electrical Engineering Department, Southwest Jiaotong University, Chengdu, China. His current research interests include machine learning, fault diagnosis, and medical image analysis.